Exome sequencing of oral squamous cell carcinoma reveals molecular subgroups and novel therapeutic opportunities

Shih-Chi Su[1,2], Chiao-Wen Lin[3,4], Yu-Fan Liu[5], Wen-Lang Fan[1], Mu-Kuan Chen[6], Chun-Ping Yu[7], Wei-En Yang[8,9], Chun-Wen Su[8,9], Chun-Yi Chuang[10,11], Wen-Hsiung Li[7], Wen-Hung Chung[1,12,13], Shun-Fa Yang[8,9,*]

[1]Whole-Genome Research Core Laboratory of Human Diseases, Chang Gung Memorial Hospital, Keelung, Taiwan; ssu1@cgmh.org.tw (Su SC); alangfan@gmail.com (Fan WL); chung1@cgmh.org.tw (Chung WH)
[2]Department of Dermatology, Drug Hypersensitivity Clinical and Research Center, Chang Gung Memorial Hospital, Linkou, Taiwan
[3]Institute of Oral Sciences, Chung Shan Medical University, Taichung, Taiwan; cwlin@csmu.edu.tw (Lin CW)
[4]Department of Dentistry, Chung Shan Medical University Hospital, Taichung, Taiwan
[5]Department of Biomedical Sciences, Chung Shan Medical University, Taichung, Taiwan yfliu@csmu.edu.tw (Liu YF)
[6]Department of Otorhinolaryngology-Head and Neck Surgery, Changhua Christian Hospital, Changhua, Taiwan 53780@cch.org.tw (Chen MK)
[7]Biodiversity Research Center, Academia Sinica, Taipei, Taiwan; chpngyu@gmail.com (Yu CP); whli@gate.sinica.edu.tw (Li WH)
[8]Institute of Medicine, Chung Shan Medical University, Taichung, Taiwan weienyang@gmail.com (Yang WE); jeff11042002@yahoo.com.tw (Su CW); ysf@csmu.edu.tw (Yang SF)
[9]Department of Medical Research, Chung Shan Medical University Hospital, Taichung, Taiwan
[10]School of Medicine, Chung Shan Medical University, Taichung, Taiwan cyi4602@yahoo.com.tw (Chuang CY)
[11]Department of Otolaryngology, Chung Shan Medical University Hospital, Taichung, Taiwan
[12]School of Medicine, College of Medicine, Chang Gung University, Taoyuan, Taiwan

*Address correspondence to: Dr. Shun-Fa Yang, Institute of Medicine, Chung Shan Medical University, 110 Chien-Kuo N. Road, Section 1, Taichung 402, Taiwan; Telephone: +886-4-24739595 ext. 34253; Fax: +886-4-24723229; E-mail: ysf@csmu.edu.tw

Supplementary Figure

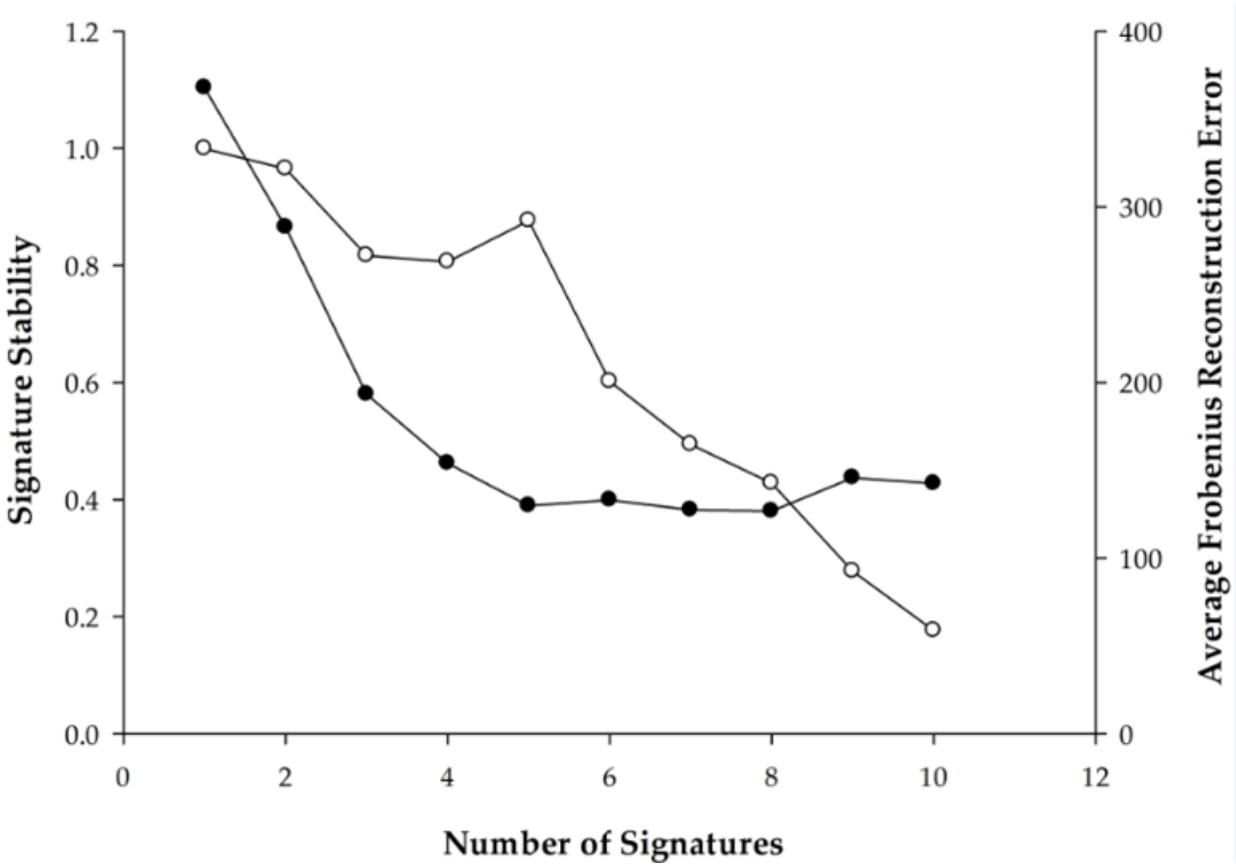

Figure S1. Determining the number of signatures operative in 120 OSCC genomes. Five signatures were extracted based on sustained reproducibility of signatures and low error for reconstructing the original catalogs.

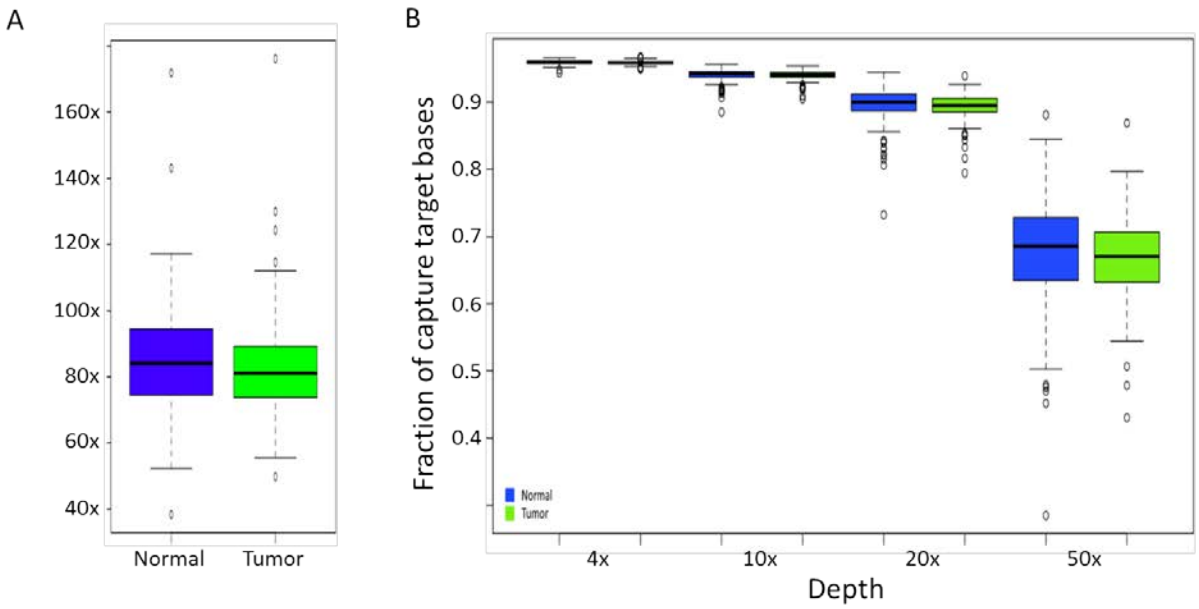

Figure S2. Sequencing depth (A) and coverage (B) in 120 tumor-normal pairs of OSCC.

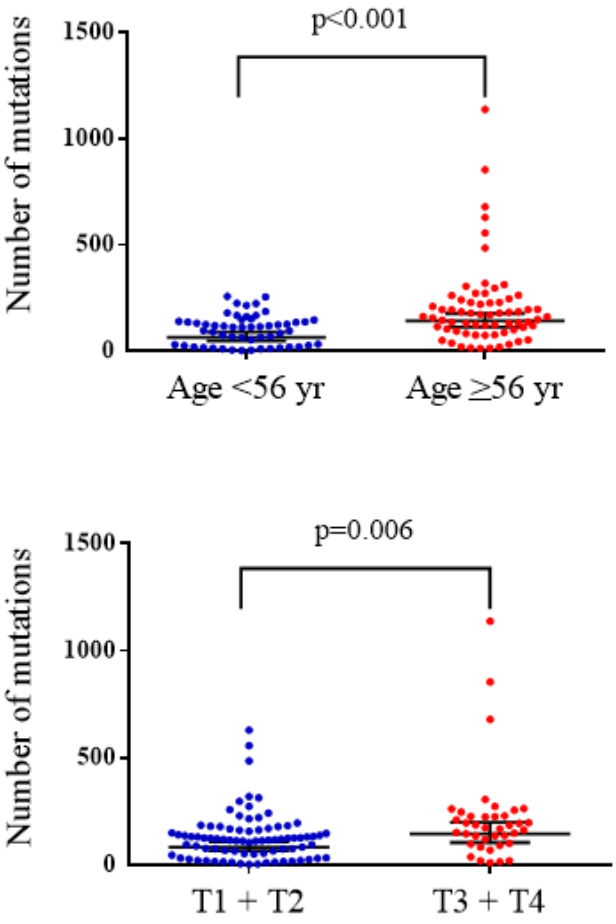

Figure S3. Number of somatic mutations in samples. Each dot represents the total somatic mutations in each sample; Student's t test was used to compare the difference between the two groups. Data represent the mean ± SD.

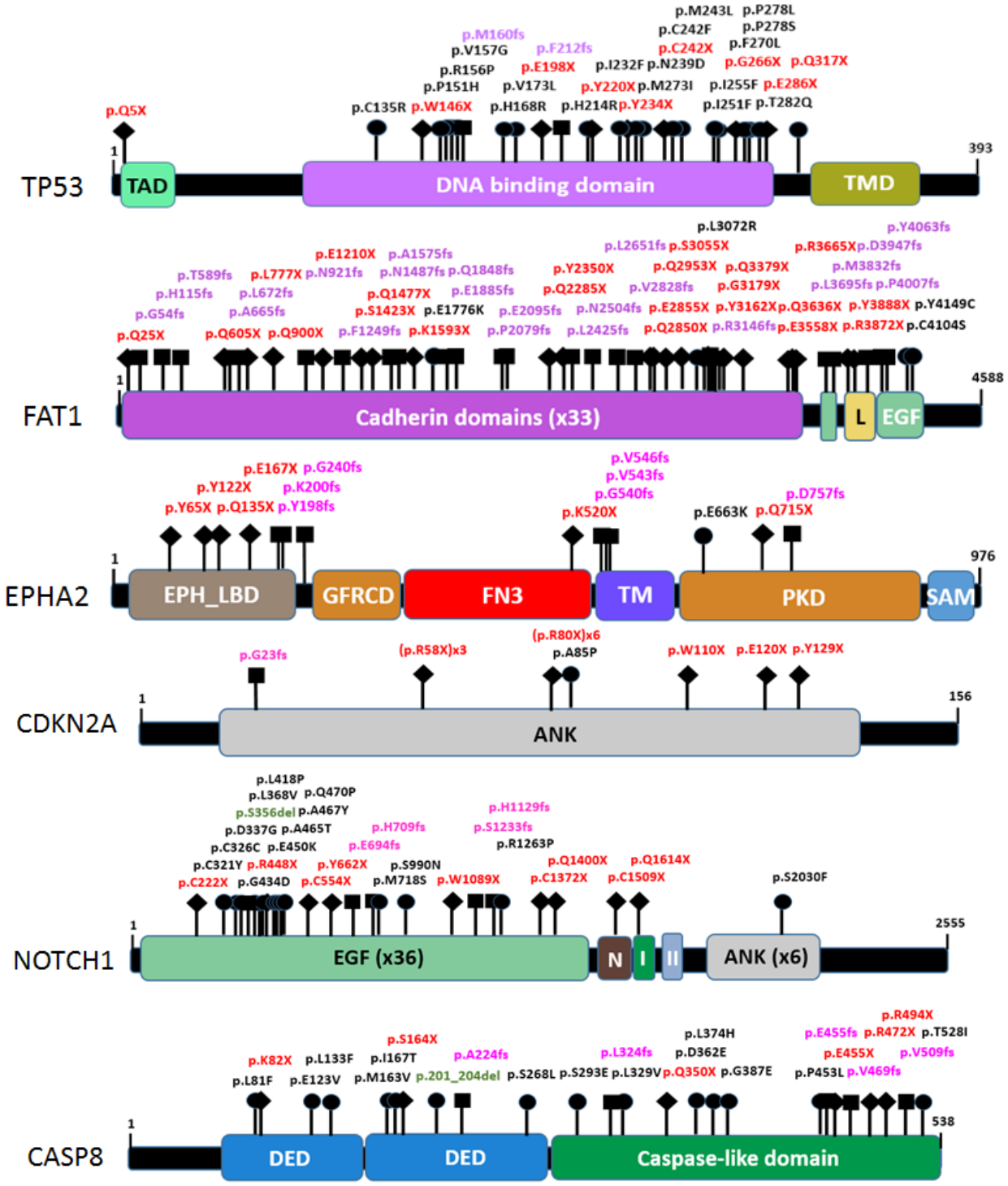
TP53
p.Q5X
p.C135R p.W146X p.H168R p.H214R p.Y234X p.I251F p.T282Q
p.M160fs p.V157G p.R156P p.P151H p.F212fs p.E198X p.V173L p.I232F p.C242F p.C242X p.N239D p.Y220X p.M273I p.M243L p.P278L p.P278S p.F270L p.G266X p.Q317X p.I255F p.E286X
1
393
TAD
DNA binding domain
TMD
FAT1
p.Q25X
p.Q605X p.Q900X p.F1249fs p.K1593X p.P2079fs p.L2425fs p.Q2850X p.R3146fs p.E3558X p.R3872X p.C4104S
p.E1210X p.A1575fs p.T589fs p.L777X p.N921fs p.N1487fs p.Q1848fs p.H115fs p.L672fs p.Q1477X p.E1885fs p.G54fs p.A665fs p.S1423X p.E1776K p.E2095fs p.Y2350X p.Q2285X p.N2504fs p.L2651fs p.S3055X p.Q2953X p.Q3379X p.V2828fs p.G3179X p.E2855X p.Y3162X p.L3072R p.R3665X p.M3832fs p.L3695fs p.Q3636X p.Y3888X p.Y4007fs p.Y4063fs p.D3947fs p.Y4149C
1
4588
Cadherin domains (x33)
L
EGF
EPHA2
p.E167X p.G240fs p.Y122X p.K200fs p.Y65X p.Q135X p.Y198fs
p.V546fs p.V543fs p.G540fs p.K520X p.E663K p.D757fs p.Q715X
1
976
EPH_LBD
GFRCD
FN3
TM
PKD
SAM
CDKN2A
p.G23fs
(p.R58X)x3
(p.R80X)x6 p.A85P
p.W110X p.E120X p.Y129X
1
156
ANK
NOTCH1
p.L418P p.L368V p.Q470P p.S356del p.A467Y p.D337G p.A465T p.H709fs p.C326C p.E450K p.E694fs p.C321Y p.R448X p.Y662X p.S990N p.C222X p.G434D p.C554X p.M718S p.W1089X p.H1129fs p.S1233fs p.R1263P p.Q1400X p.Q1614X p.C1372X p.C1509X p.S2030F
1
2555
EGF (x36)
N
I
II
ANK (x6)
CASP8
p.K82X p.L133F p.I167T p.S164X p.A224fs p.L81F p.E123V p.M163V p.201_204del p.S268L p.S293E p.L324fs p.L329V p.L374H p.D362E p.Q350X p.G387E p.R494X p.E455fs p.R472X p.T528I p.E455X p.V509fs p.P453L p.V469fs
1
538
DED
DED
Caspase-like domain

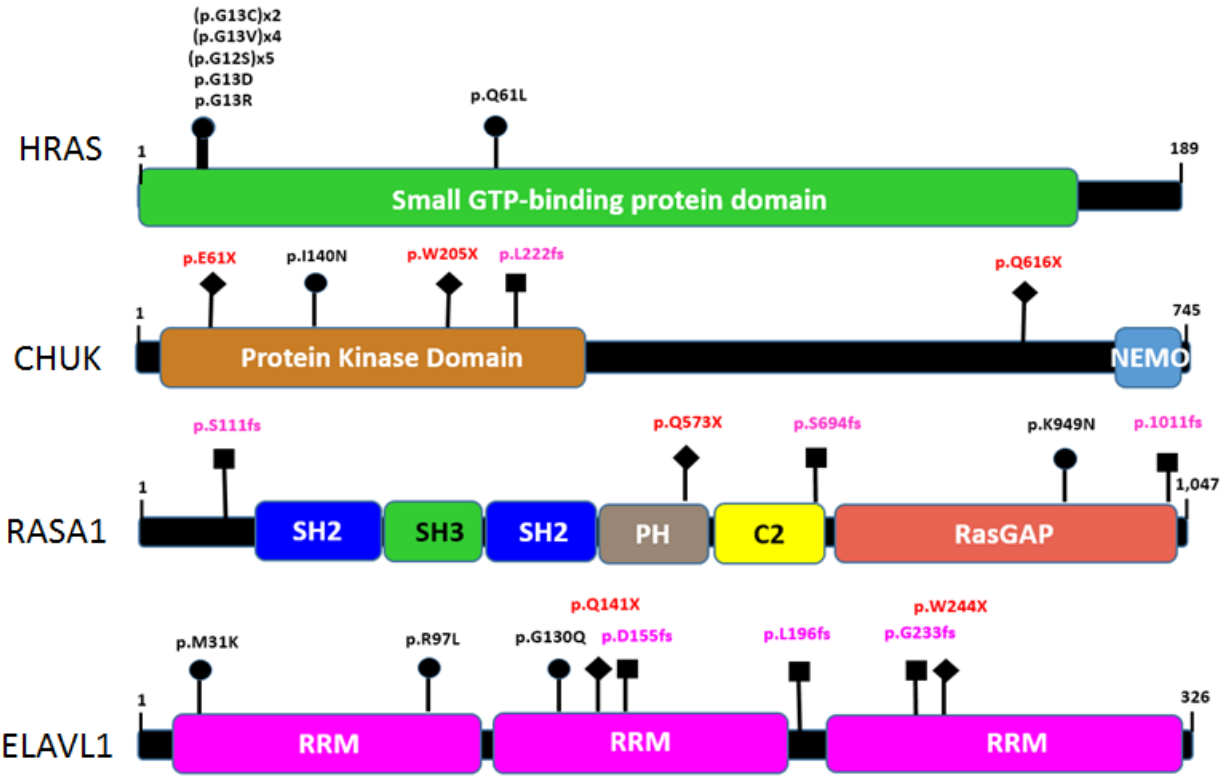

Figure S4. Distribution of protein-altering mutations in significantly mutated OSCC driver genes. Schematic diagram of domains organization of putative drivers generated by InterPro database including TAD (transactivation domain), DNA binding domain and TMD (tetramerization domain) in TP53 (P04637); 33 tandem Cadherin domains, 4 EGF (EGF-like domain and L (Laminin G domain) in FAT1; EPH_LDB (Ephrin receptor ligand binding domain), GFRCD (Growth factor receptor cysteine-rich domain), FN3 (Fibronectin type III domain), TM (transmembrane domain), PKD (protein kinase domain) and SAM (Sterile alpha motif domain) in EPHA2 (P29317); ANK (Ankyrin repeat-containing domain) in CDKN2A (P42771); 36 tandem EGFs, N (Notch domain), I (Notch, NOD domain), II (Notch, NODP domain) and 6 tandem ANK in NOTCH1 (P46531); 2 tandem DEDs (Death Effector Domains) and Caspase-like domain in CASP8 (Q14790); ABD (adaptor-binding domain), RBD (Ras-binding domain), C2 ($Ca2^{+}$-dependent membrane-targeting module), PIK (accessory domain) and Kinase domain

in PIK3CA (P42336); Small GTP-binding protein domain in HRAS (P01112); PKD (Protein Kinase domain) and NEMO (I-kappa-kinase NEMO binding domain) in CHUK (O15111); 2 SH2 (Src homology 2), SH3 (Src homology 3), PH (Pleckstrin homology), C2 and RasGAP (Ras GTPase-activating protein) in RASA1 (P20936); 3 tandem RRM (Eukaryotic RNA Recognition Motif) in ELAVL1 (Q15717); Each bar represents a somatic mutation in OSCC. Types of mutation are highlighted as: (●) missense, color black; (◆) nonsense, color red; (■) frameshift, color purple; (●) in-frame deletion, color green.

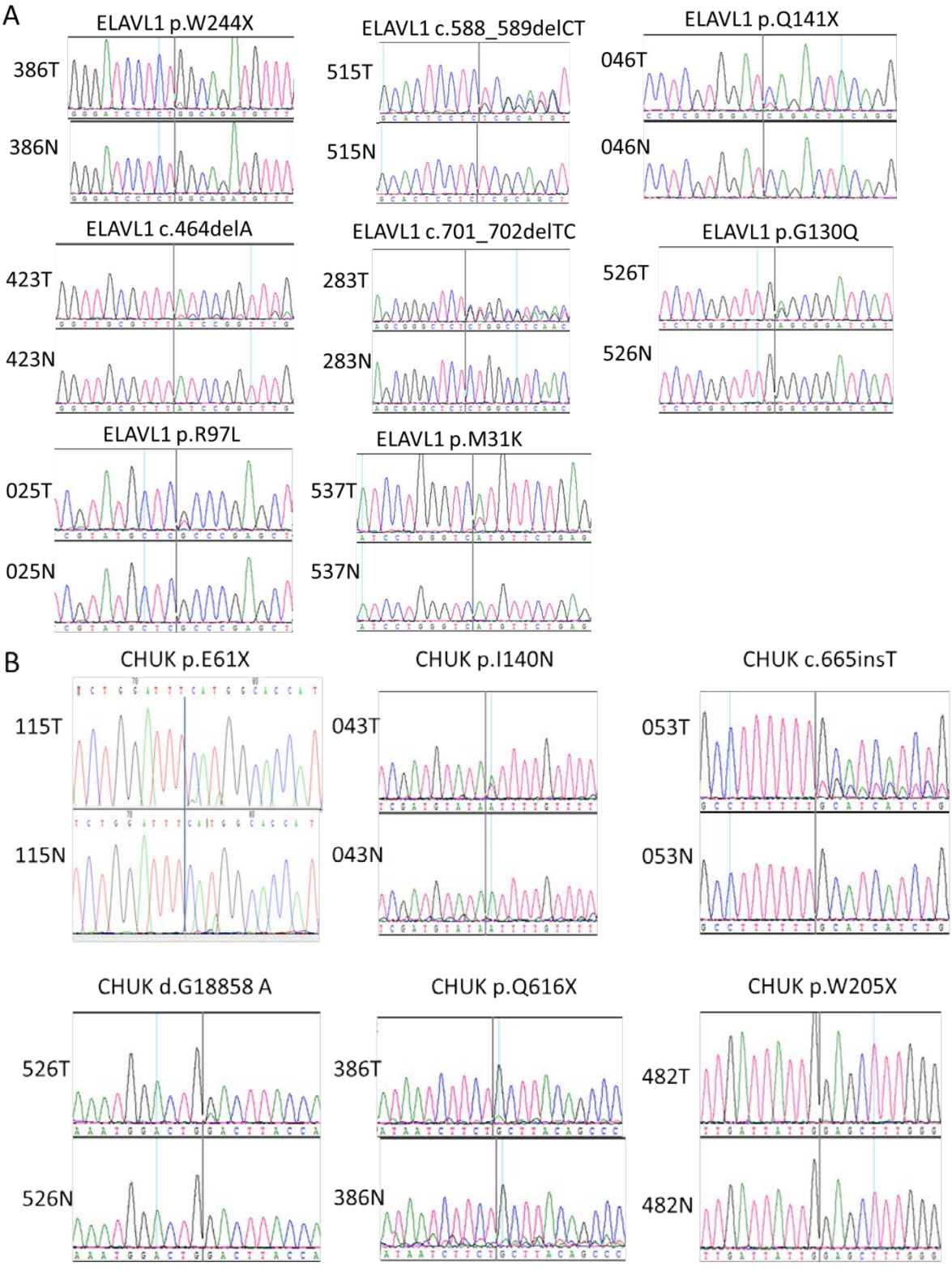
A
ELAVL1 p.W244X
386T
386N
ELAVL1 c.588_589delCT
515T
515N
ELAVL1 p.Q141X
046T
046N
ELAVL1 c.464delA
423T
423N
ELAVL1 c.701_702delTC
283T
283N
ELAVL1 p.G130Q
526T
526N
ELAVL1 p.R97L
025T
025N
ELAVL1 p.M31K
537T
537N
B
CHUK p.E61X
115T
115N
CHUK p.I140N
043T
043N
CHUK c.665insT
053T
053N
CHUK d.G18858 A
526T
526N
CHUK p.Q616X
386T
386N
CHUK p.W205X
482T
482N

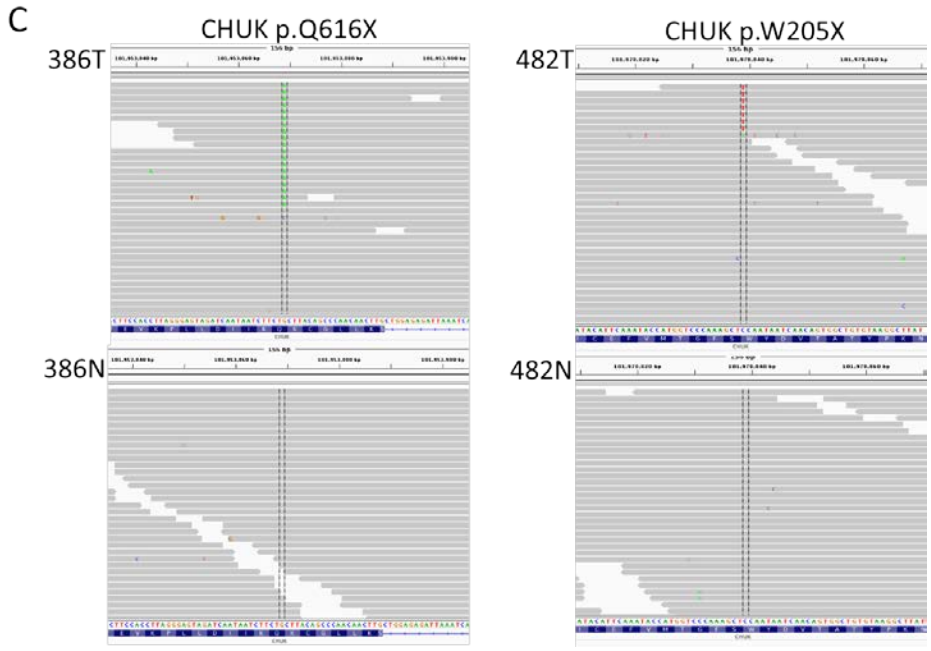

Figure S5. Validation of mutations via Sanger sequencing. **(A)** Sanger sequencing of tumors harboring *ELAVL1* somatic mutations. **(B)** Sanger sequencing of tumors carrying *CHUK* somatic mutations. **(C)** Alignment of *CHUK* mutations (p.Q616X and W205X) from IGV (Intergative Genomics Viewer) are shown.

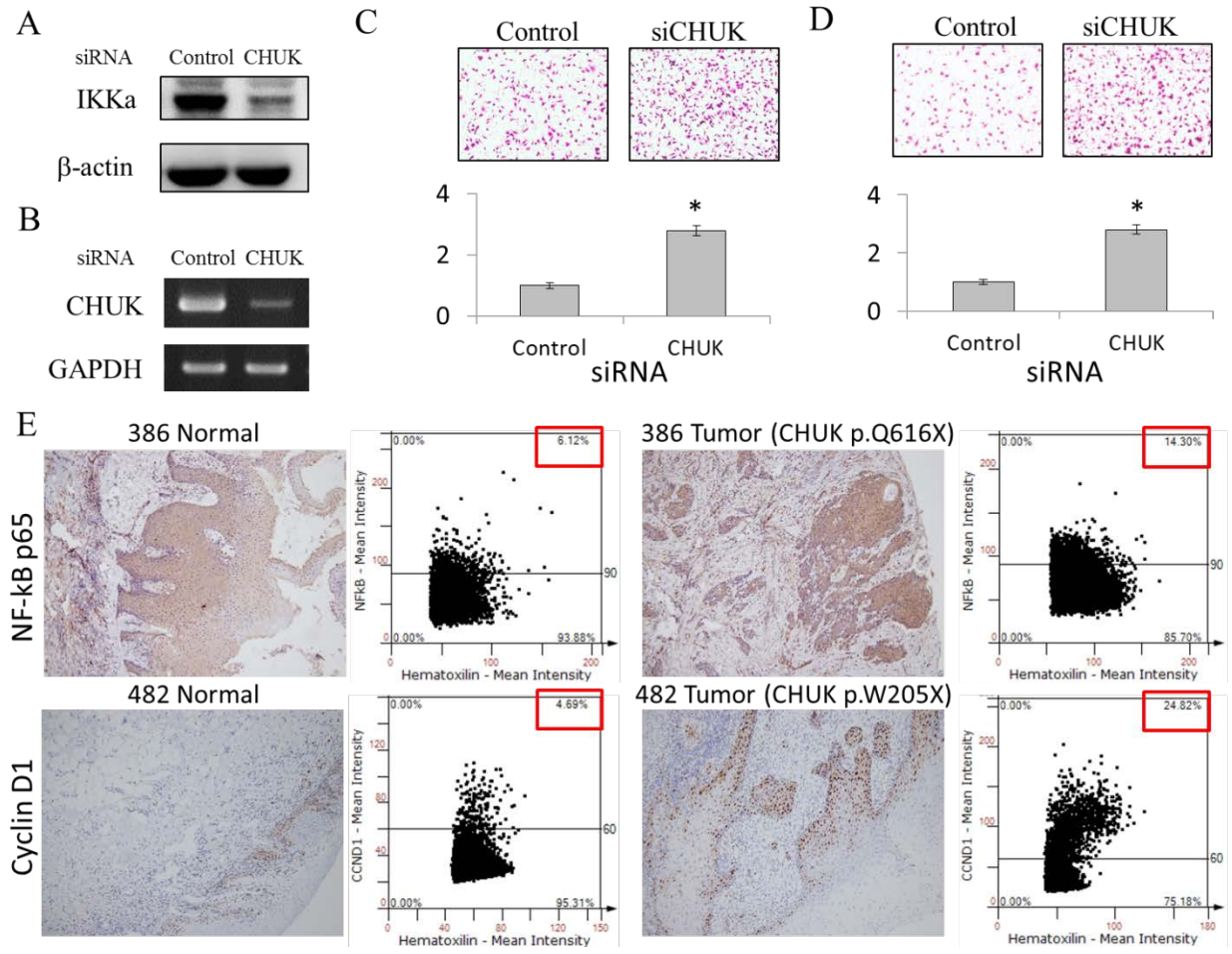

Figure S6. The effect of gene silencing was verified on the protein and mRNA level by immunoblotting **(A)** and RT-PCR **(B)**, respectively. Cell migration **(C)** and invasion **(D)** of SCC-9 were measured by using a modified Boyden chamber assay. Data presented are average values of relative responses ± S.D. from representative experiments (n=4, Student's t test; *, p 0.05, compared with controls). **(E)** Immunohistochemical staining of OSCC harboring *CHUK* mutations. Human OSCC specimens and normal counterparts were stained using specific antibodies against cyclin D1 and NF-κB p65. The right panels are quantitative analyses of staining intensities.

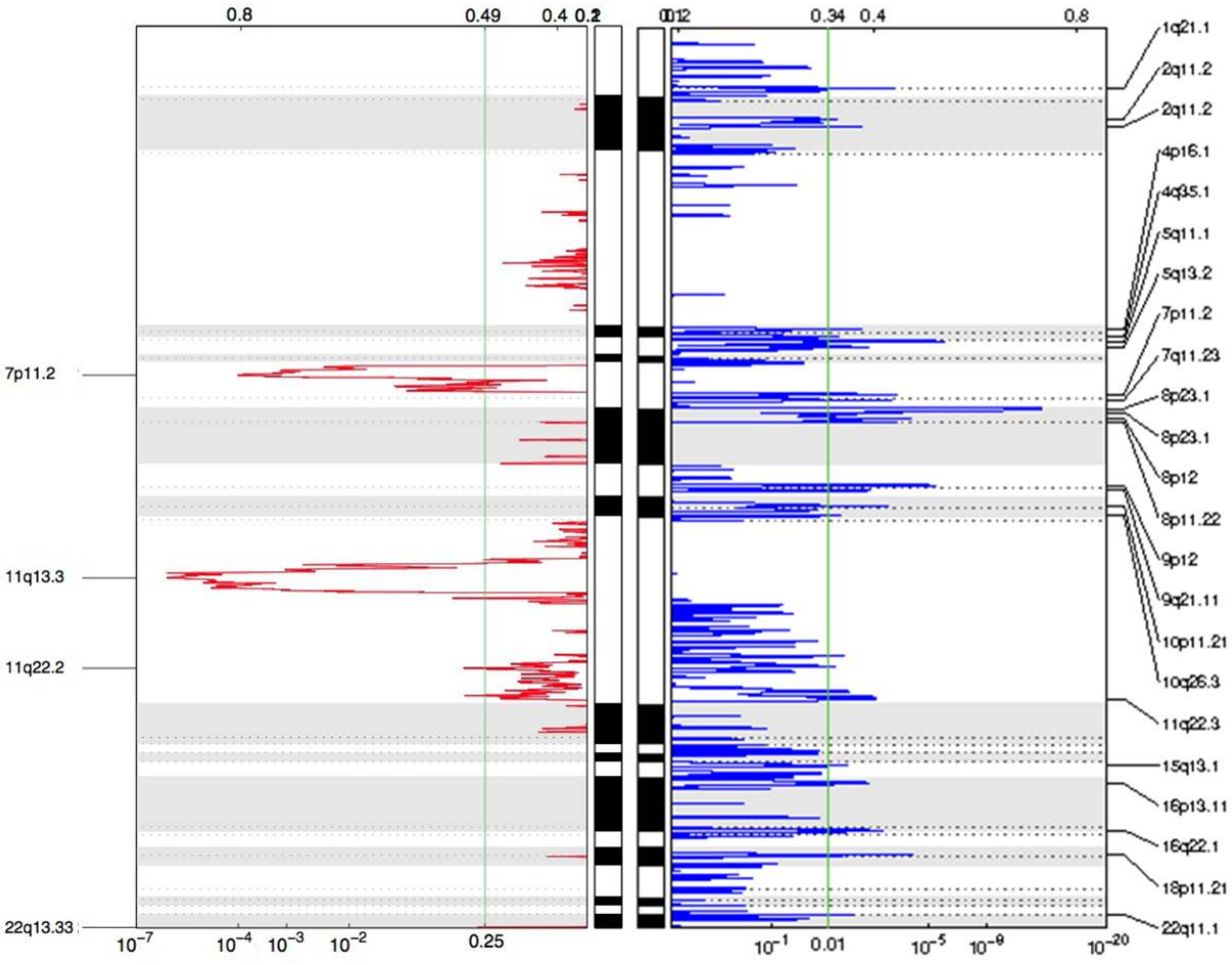

Figure S7. GISTIC analysis of focal copy-number alterations. Copy-number gains were shown in red and losses in blue. Significant regions (Q-value <0.25) were indicated by the cytoband location.

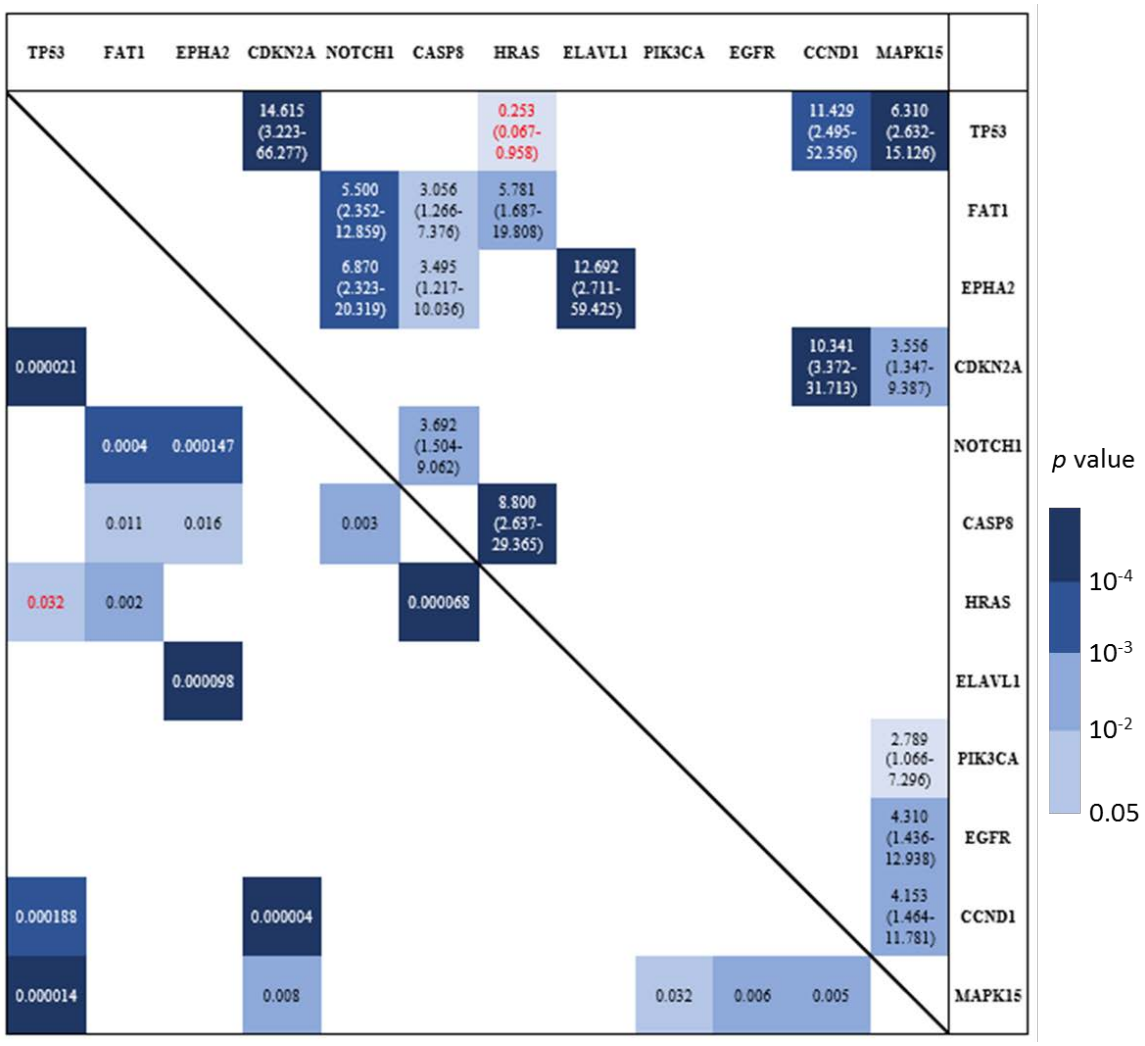

Figure S8. Association between gene alterations. Chi square contingency table test was performed and p-value was shown in the lower half as well as in blue color. The strength of association or exclusion among gene alteration events was shown in the upper half.

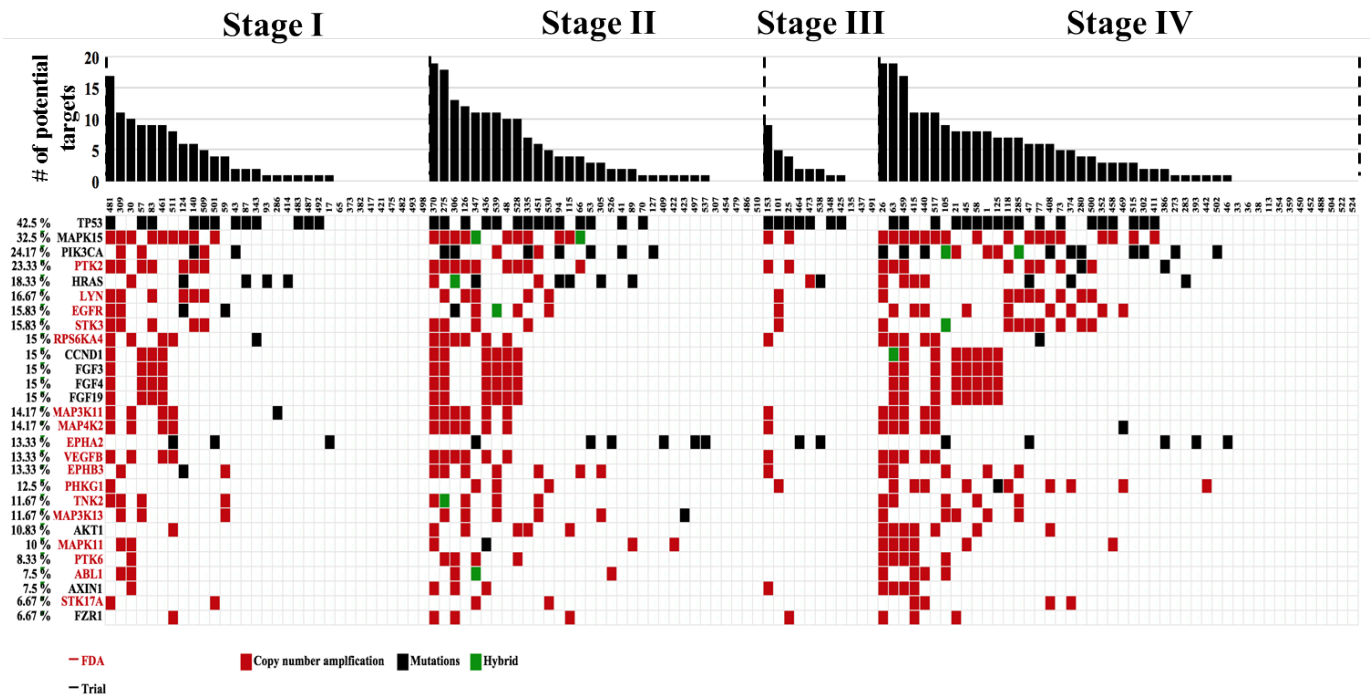

Figure S9. Distribution of actionable events per sample. Gene names marked in red and black are targets of FDA-approved agents and drugs screened in clinical trials, respectively. Data have been organized in decreasing order of the total number of targetable events in each patient.

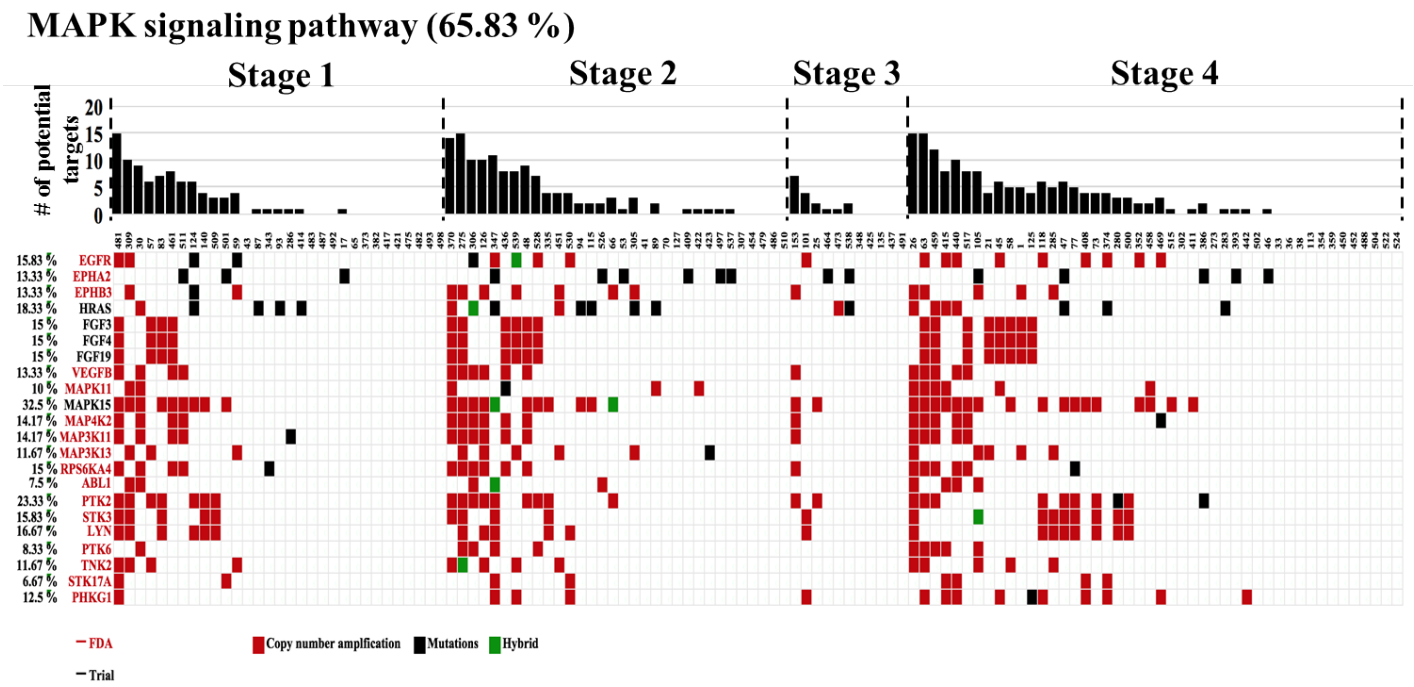

Figure S10. Mutational spectrum of the MAPK pathway.

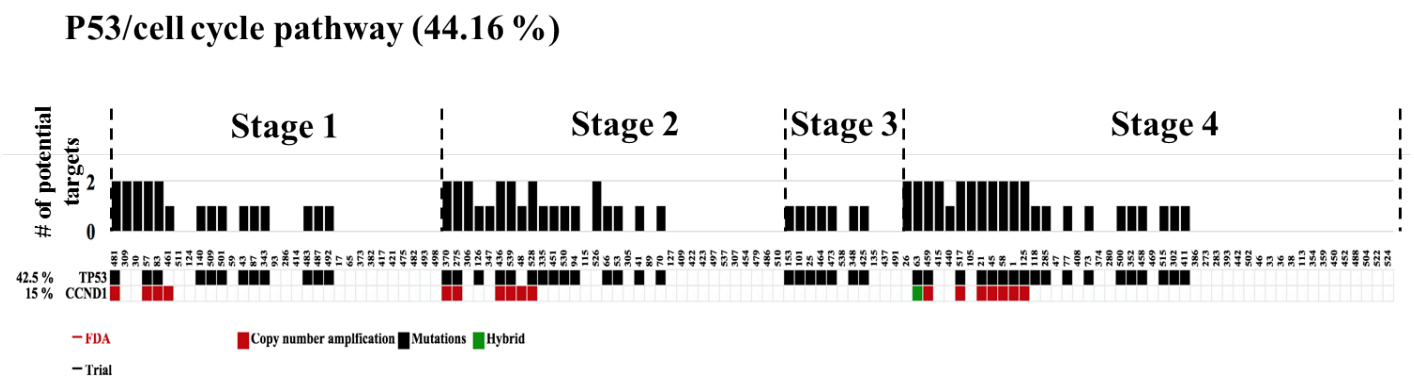

Figure S11. Mutational spectrum of the p53/cell cycle pathway.

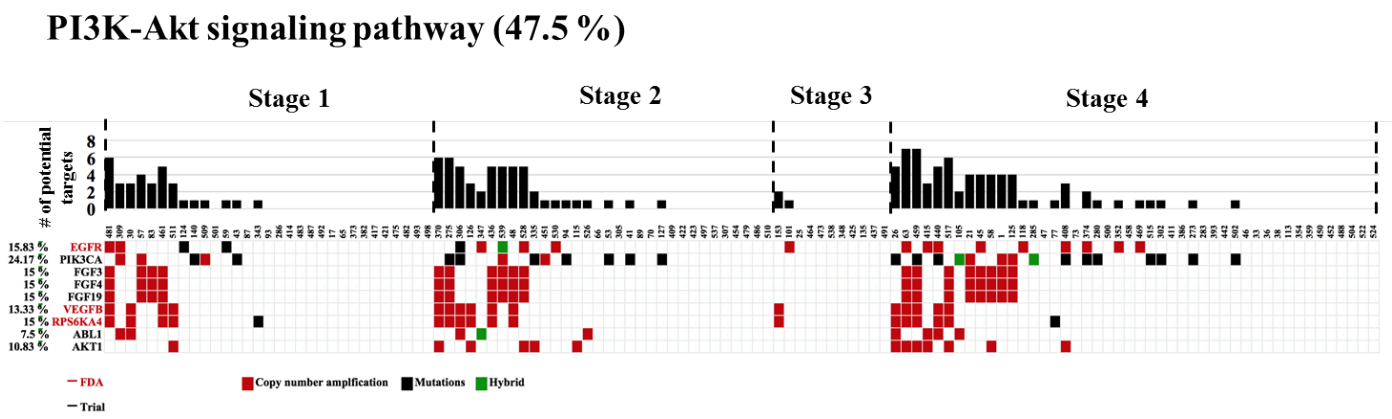

Figure S12. Mutational spectrum of the PI3K-Akt pathway.

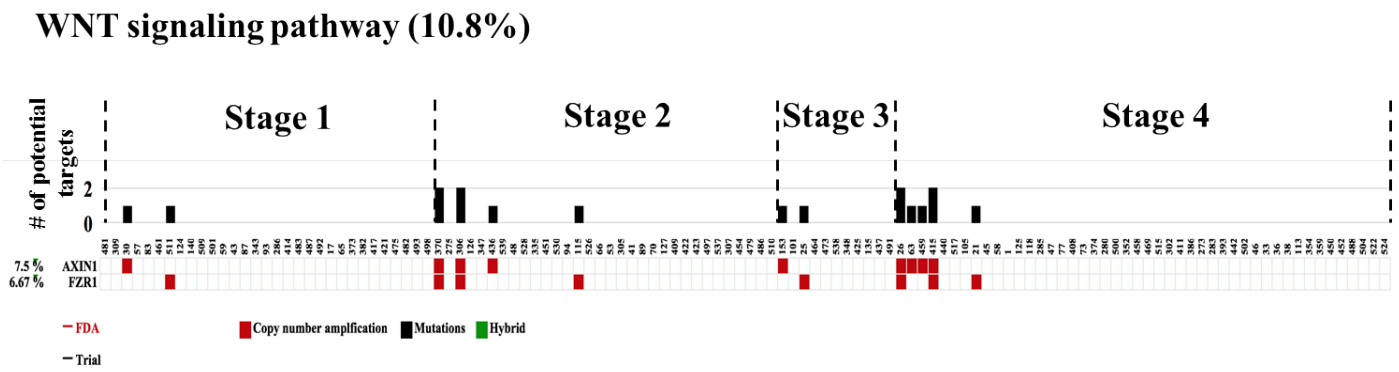

Figure S13. Mutational spectrum of the Wnt signaling pathway.

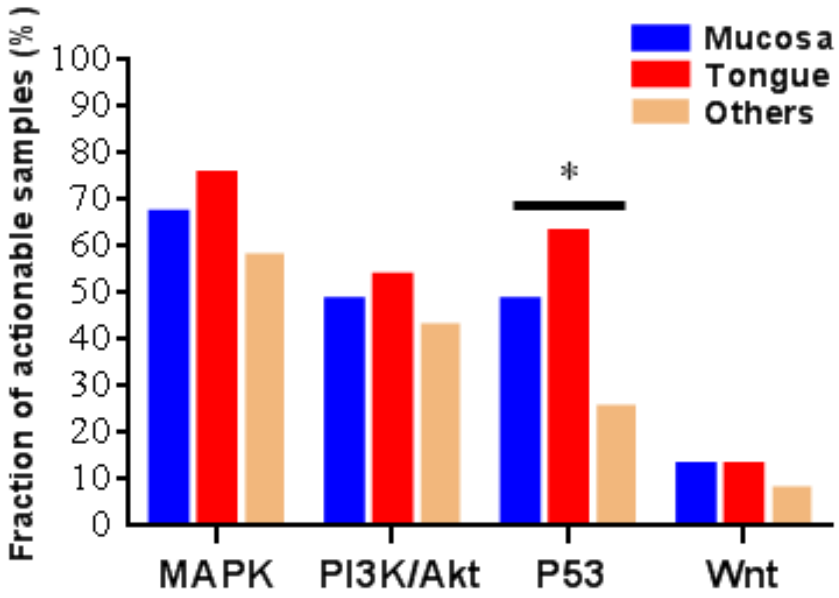

Figure S14. Distribution of actionable tumors at different anatomical sites targeted against different pathways. *$p < 0.05$, $\chi 2$ test.

T393

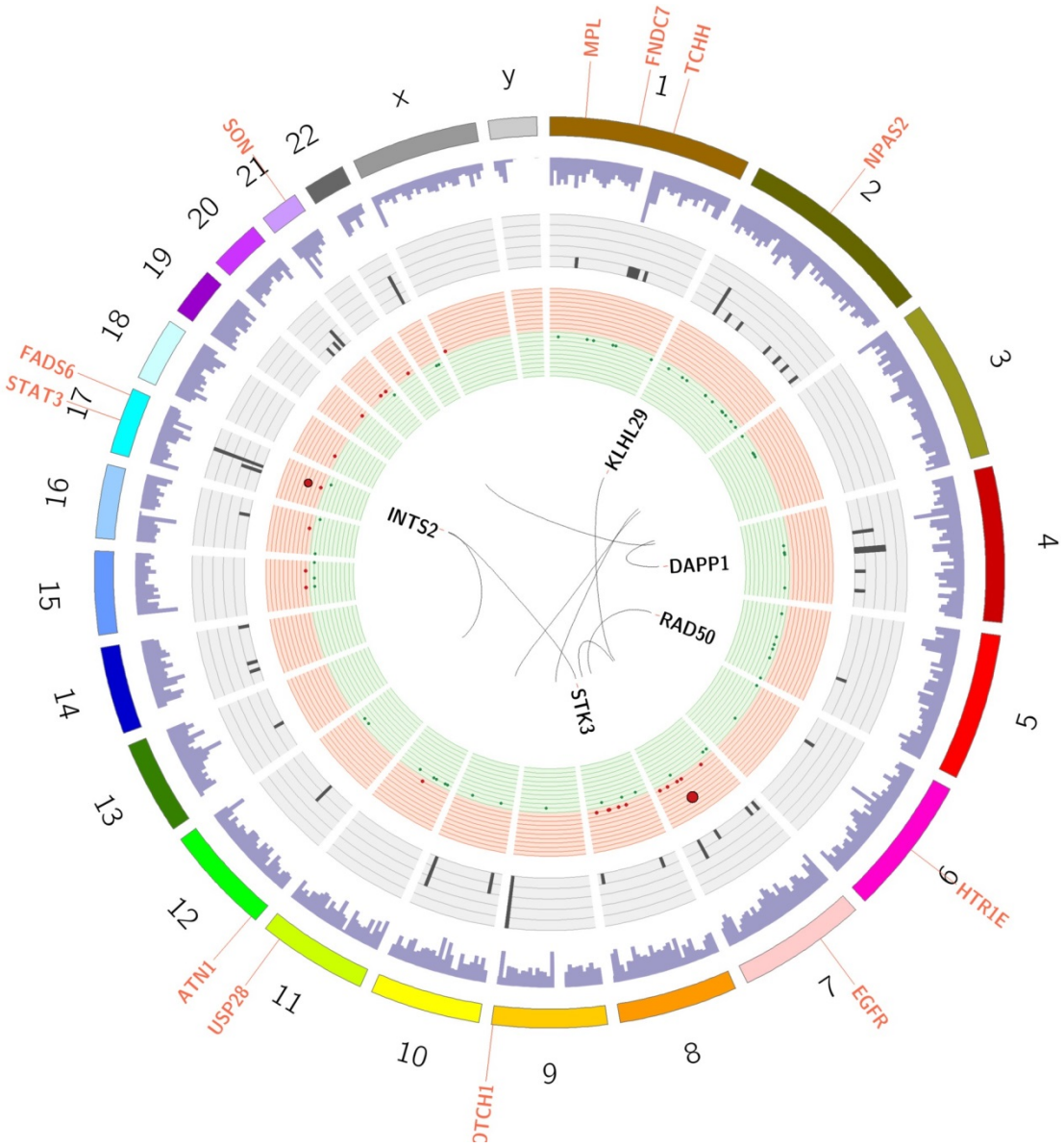
MPL
FNDC7
TCHH
NPAS2
SON
FADS6
STAT3
KLHL29
INTS2
DAPP1
RAD50
STK3
HTR1E
EGFR
ATN1
USP28
PTCH1

T491

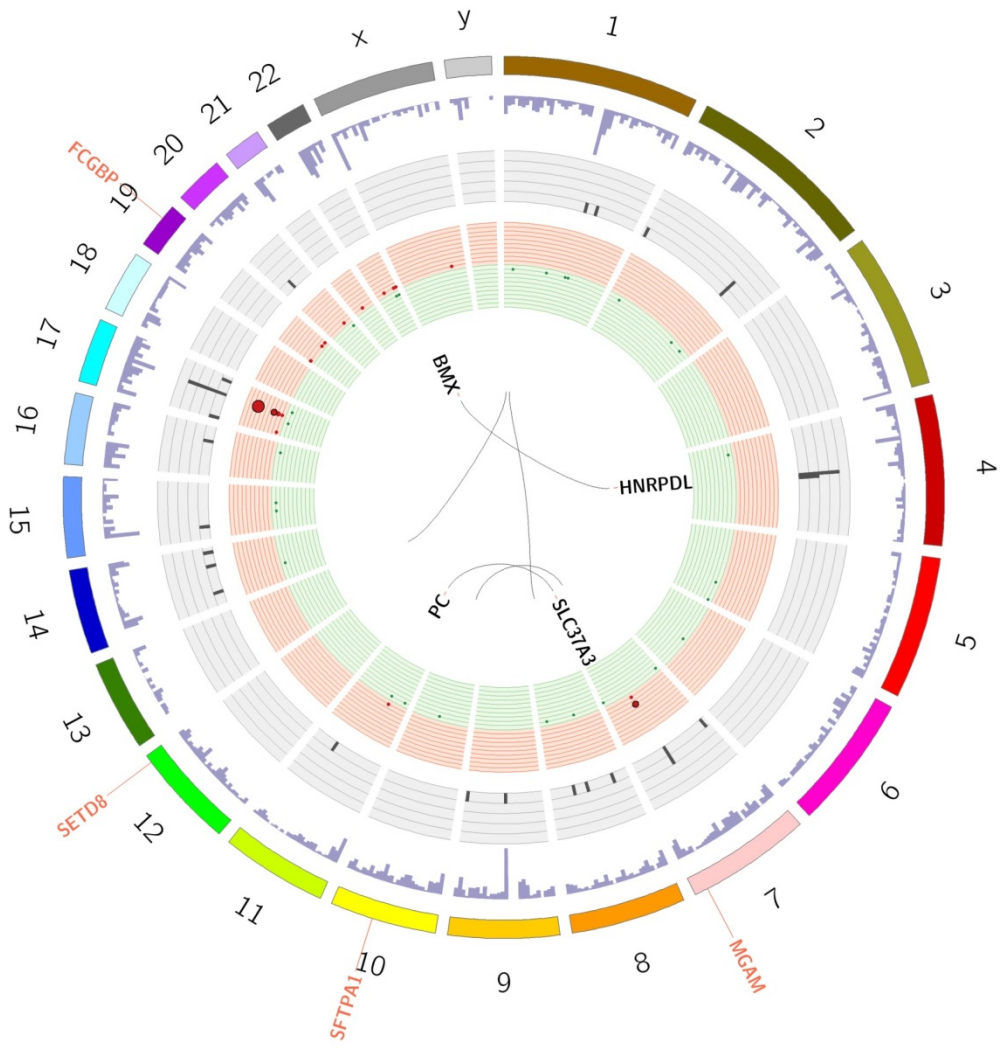

Figure S15. Circos plots of somatic SNVs, INDELs, copy-number variations (CNVs), and structural variations (SVs) in two OSCC genomes. The inner ring displays SVs: black lines for interchromosomal SVs. The second ring next to SVs is CNV: green dots for copy loss and red dots for copy gain. The third ring is INDELs, shown in gray. The fourth ring is SNVs, shown in purple. The outside ring is the chromosome ideogram. Genes in red shown on the outside of rings represent the genes detected both in our data and in cosmic database.

Table S1. Similarities between the signatures in this study and COSMIC dataset.

OSCC	COSMIC (Alexandrov *et al.*)	Cosine similarity
Signature I	Signature 13	0.86
Signature II	Signature 7	0.95
Signature III	Signature 1	0.95
Signature IV	Signature 6	0.90
Signature V	Signature 5	0.89

Table S2. Primer sequence and TaqMan assays for Sanger sequencing and quantitative PCR

Gene	Chromosome number	Primer name	product size	Sequence (5’ to 3’)
ASXL1	20	ASXL-1F	210	AAAGTGGCTTGTGTGTCCCA
ASXL1	20	ASXL-1R	210	CCCCATCCTTGTAGAGGGGA
ASXL1	20	ASXL-2F	670	GACTCACACAGTCCCACCAG
ASXL1	20	ASXL-2R	670	AGCTCTGGACATGGCAGTTC
CHRNB4	15	CHRNB4-1F	377	CTTTATCCCCATTGCCCGGT
CHRNB4	15	CHRNB4-1R	377	CATGTTTGTGTGCGTCCTGG
CHRNB4	15	CHRNB4-2F	461	GGCTCTGCTCACCTCTGTTT
CHRNB4	15	CHRNB4-2R	461	GCTCCTCCTTCCTGGTGAAC
CHRNB4	15	CHRNB4-3F	335	ACCCAGCTGAGCAGAGTCTA
CHRNB4	15	CHRNB4-3R	335	GCTCCTCACAGCTCATCTCC
CHUK	10	CHUK-1F	375	GTCTGGACACCAAGCAAGGA
CHUK	10	CHUK-1R	375	CCTCAGCTGGGTTTTGGGAA
CHUK	10	CHUK-2F	297	TCCTGTGAGAGCCCTATCCT
CHUK	10	CHUK-2R	297	AAGGGCCATTTGCTTCCAGA
CHUK	10	CHUK-3F	311	GCATGCCCAAGTTCTCATCC
CHUK	10	CHUK-3R	311	TGGGAACACTGCAGTATCTGG
CHUK	10	CHUK-4F	785	GCAGGTGCTGTTCCTTCTCT
CHUK	10	CHUK-4R	785	CACCCAGCCAAGTCAACTCT
CHUK	10	CHUK-5F	128	AGAGTGGATTCCTGGCCTCT
CHUK	10	CHUK-5R	128	AAAACAGAGAACGATGGTGCC
ELAVL1	19	ELAVL1-1F	368	TGGTCACAAAGCCAAACCCT
ELAVL1	19	ELAVL1-1R	368	GACCCATGCAGGTGTCTCAA
ELAVL1	19	ELAVL1-2F	551	TCTATTCTGTGGCTGTGCCG
ELAVL1	19	ELAVL1-2R	551	TATCTTTGGGCGCCAACACT
ELAVL1	19	ELAVL1-3F	502	CCTAGAGAACACCCTCCCCA
ELAVL1	19	ELAVL1-3R	502	AGAGGTAGCCACACACAAGC
ELAVL1	19	ELAVL1-4F	499	GGACCCAATCAATCTGCCCA
ELAVL1	19	ELAVL1-4R	499	GAAGACCACATGGCCGAAGA
EPHA2	1	EPHA2-1F	710	TTCTGCCTCCTGAAGCACTG
EPHA2	1	EPHA2-1R	710	CCCTCCTCCCCAATACCTGA
EPHA2	1	EPHA2-2F	1309	AGAGGTAATGACCCCCGTGT
EPHA2	1	EPHA2-2R	1309	GCCATCTGAAGAAGCACCCT
EPHA2	1	EPHA2-3F	459	CAGGAGGAGTCAGTGCTGTG
EPHA2	1	EPHA2-3R	459	TTGCAGCATGTGTGTGAAGC
EPHA2	1	EPHA2-4F	726	ACCAGAACCTGGGAATGCAG
EPHA2	1	EPHA2-4R	726	GTGGGACCTGATGCAGAACA
RPTN	1	RPTN-1F	315	CCCACATGGACCTTCCTGAC
RPTN	1	RPTN-1R	315	GTCAGGAAGGTCCATGTGGG
RPTN	1	RPTN-2F	300	TAGCCTGGCCACTGGTAGAT
RPTN	1	RPTN-2R	300	AACACAGACAGAGGCACGAG
TP53	17	TP53-1F	338	GCATGTTGCTTTTGTACCGTCA
TP53	17	TP53-1R	338	CTGGGACCCAATGAGATGGG

TP53	17	TP53-2F	1376	GGGCTTTCTCCTGCTGCTTA
TP53	17	TP53-2R	1376	TCTTTGAGGCATCACTGCCC
TP53	17	TP53-3F	590	CTAGTGGGTTGCAGGAGGTG
TP53	17	TP53-3R	590	TAAGCAGCAGGAGAAAGCCC
TP53	17	TP53-4F	851	AGTGCTTGGGTTGTGGTGAA
TP53	17	TP53-4R	851	AAGTCTCATGGAAGCCAGCC
CASP8	2	CASP8-1F	1068	ACCACACTCTGGTCACAACC
CASP8	2	CASP8-1R	1068	TCTCTAGGGTGGGGAGAAGC
CASP8	2	CASP8-2F	1560	TCACCACACCAGCCTCTTTC
CASP8	2	CASP8-2R	1560	GGCTGCTGCTTCTCTCTGAA
CASP8	2	CASP8-3F	820	ATTGCCCTGCTTGCAGAATC
CASP8	2	CASP8-3R	820	TATTACCCCCTCCACCCTCC
CASP8	2	CASP8-4F	1083	CCTCAGCTGTTAGCCACGAA
CASP8	2	CASP8-4R	1083	TGGCTGAGCAAAAGAATTGC
CASP8	2	CASP8-5F	716	CTCTCCAGCTGTGGTCTGTG
CASP8	2	CASP8-5R	716	CCACTCCCCTTGGACAGTTC
CASP8	2	CASP8-6F	736	GCACAGCAGAGGAGACAGTT
CASP8	2	CASP8-6R	736	GCTGGATTTTGTACGTGTCTGG

Gene	**Assay ID**
ANO1	Hs02564912_cn
FADD	Hs06260438_cn

Table S3. Demographic characteristics and clinical features of OSCC patients

Variables	OSCC (n = 120)
Age (years)	56.13 ± 10.79
<40	8 (6.7%)
40-49	24 (20.0%)
50-59	43 (35.8 %)
60-69	31 (25.8%)
≥70	14 (11.7 %)
Smoking status	
No	13 (10.8%)
Yes	107 (89.2%)
Drinking status	
No	60 (50.0%)
Yes	60 (50.0%)
Betel nut chewing	
No	25 (20.8%)
Yes	95 (79.2%)
Cancer location	
Buccal mucosa	48 (40.0%)
Tongue	32 (26.7 %)
Lip	12 (10.0 %)
Gingiva	11 (9.2 %)
Others	17 (14.1 %)
Stage	
I	31 (25.8%)
II	32 (26.7%)
III	11 (9.2%)
IV	46 (38.3%)
Tumor T status	
T1	39 (32.5%)
T2	42 (35.0%)
T3	5 (4.2%)
T4	34 (28.3%)
Lymph node status	
N0	84 (70.0%)
N1	12 (10.0%)
N2	24 (20.0%)
Metastasis	
M0	120 (100%)
M1	0 (0%)
Cell differentiation	
Well	22 (18.3%)
Moderately	88 (73.4%)
Poorly	10 (8.3%)

Table S4. Statistics of various parameters pertaining to somatic mutations

Statistic	Minimum	Maximum	Median	Mean±SE
Total No. of mutations	3	1146	129	160.72±14.67
Total no. of mutations, excluding synonymous mutations	2	950	107	130.84±12.12
Ratio of non-synonymous to synonymous mutations	0	4.22	2.28	2.22±0.08
Mutation rate per Mb	0.05	19.14	2.15	2.64±0.24
Mutation rate per Mb, excluding synonymous mutations	0.03	15.86	1.79	2.18±0.2

Table S5. Distributions of somatic mutations

Categories	SNV	INDEL
UTR5;UTR3	**1**	**-**
exonic;splicing	**1**	**-**
ncRNA_exonic;splicing	**1**	**-**
ncRNA_splicing	**3**	**-**
upstream;downstream	**9**	**-**
downstream	**30**	**-**
upstream	**62**	**-**
splicing	**162**	**4**
ncRNA_exonic	**238**	**9**
UTR5	**248**	**10**
ncRNA_intronic	**270**	**14**
UTR3	**285**	**19**
intergenic	**528**	**11**
intronic	**4701 (26%)**	**267 (34%)**
exonic	**11232 (63%)**	**453 (58%)**
Total	**17771**	**787**

Table S6. Functional annotations of somatic mutations

Categories	SNV	INDEL
stoploss	**9**	**-**
unknown	**128**	**2**
stopgain	**551**	**15**
synonymousSNV	**3196**	**-**
nonsynonymousSNV	**7349**	**-**
nonframeshift Insertion	**-**	**20**
nonframeshift Deletion	**-**	**70**
frameshift Insertion	**-**	**106**
frameshift Deletion	**-**	**240**
others	**6538**	**334**
Total	**17771**	**787**

Table S7. Genes frequently but not significantly mutated in OSCC

Gene	MutSigCV q value	intOGen q vlaue	Chi-Square q value	Patients number (%)	Gene size (KB)	Protein size (AA)
TTN	1	ND	0.779955677	34 (28.33%)	305	34350
PCLO	1	0.639027389	0.779955677	20 (16.67%)	409	5065
CSMD3	1	ND	0.779955677	17 (14.17%)	1214	3707
MUC16	1	ND	0.779955677	15 (12.5%)	132	22152
MUC5B	1	ND	0.779955677	13 (10.83%)	39	5762
MUC4	1	1	0.779955677	11 (9.17%)	65	2169
MLL3	1	1	ND	10 (8.33%)	302	4911
USH2A	1	ND	0.98522	10 (8.33%)	800	5202

Supplementary Materials and Methods

Immunohistochemistry

Immunohistochemical analyses were performed on formalin-fixed, paraffin-embedded tissue sections using VECTASTAIN Universal Elite ABC Kit (Vector Labs). High pH Antigen Unmasking Solution (Vector Labs) was used to heat tissue sections for antigen retrieval and the Avidin/Biotin Blocking Kit (Vector Labs) was utilized to avoid nonspecific background before the first antibody hybridization. Primary antibodies against NF-κB p65 (sc-109, Santa Cruz Biotechnology) and cyclin D1 (MA5-16356, Thermo Fisher Scientific) were used to assess protein expression on clinical specimens. Photographs were taken under a Nikon Eclipse Ti-U inverted microscope equipped with a CCD camera and NIS-Elements imaging software. Quantitative analysis was performed by the HistoFAXS software (TissueGnostics).

Cell culture and silencing of *CHUK*

SCC-9 cells were obtained from Bioresource Collection and Research Centre (BCRC), Taiwan. Cells that have been tested for mycoplasma contamination were cultured in RPMI 1640 (Gibco) supplemented with 10% fetal bovine serum (FBS). Cells were transfected with 1.5 nM short interfering RNA (siRNA) directed to CHUK (s3077, Ambion) or a non-target control (Select Negative Control No. 1 siRNA) using Lipofectamine RNAiMAX (Invitrogen) according to the manufacturer's protocol.

Immunoblotting

Cell extracts were prepared by lysis in RIPA buffer supplemented with 1 mM PMSF, 10 mg/ml leupeptin, and 10 mg/ml aprotinin. Samples were separated using SDS-PAGE gels and transferred to polyvinylidene difluoride (Millipore). Antibodies against the following proteins were used for detection: IKK alpha (ab54628, abcam) and beta-actin (ab8229, abcam).

RT-PCR

Total RNA was isolated from SCC-9 cells by using REzol® C & T as per manufacturer's instruction. Random hexamer was used for reverse transcription, and PCR was carried out by using primers listed below. CHUK-forward, 5'-TGAGGAACAGGGCAATAGTATGATG-3'; CHUK-reverse, 5'-GGTCTTACGCCCAAAAGTTAAAAGT-3'; GAPDH-forward, 5'- CGGAG

TCAACGGATTTGGTCGTAT-3'; GAPDH-reverse, 5'-AGCCTTCTCCATGGTTGGTGAAGAC-3'.

Migration and invasion assay

Migration and invasion assays were performed as described (1). In brief, after treatment with siRNA for 48 hr, cells were assayed in Boyden chambers with 6.5-mm diameter polycarbonate membrane filters containing 8 mm pore size (Neuro Probe) at 10^4 cell/well in serum-free medium and incubated for 24 hr. For invasion assay, membrane filters were covered with 10 ul of Matrigel (25 mg/50ml, BD Biosciences) and air-dried for 5 hr. Cell were allowed to invade into the bottom chamber containing DMEM-F12 medium with 10% FBS for 24 hr. Invading cells were fixed with 100% methanol and stained with 5% Giemsa and counted under a light microscope. Data were representative of three independent experiments.

Detection of somatic structural variants

Analysis of structural variants (SVs) was performed by CREST (2) using the default parameters. Candidate breakpoints in tumors that also appeared in the paired normal specimens were removed before the final SV detection step was performed. Candidate SVs were called by the following filtering criteria: 1) if both breakpoints fell within a repeat region, 2) if any of the breakpoints were located within <1kb of a known assembly gap region within the reference genome, 3) mean read depth of at least 10 reads across the event. The remaining set of somatic SVs was annotated with gene information.

Reference

1. Yang SF, Chen MK, Hsieh YS, Yang JS, Zavras AI, Hsieh YH, et al. Antimetastatic effects of Terminalia catappa L. on oral cancer via a down-regulation of metastasis-associated proteases. Food and chemical toxicology : an international journal published for the British Industrial Biological Research Association. 2010 Apr;48(4):1052-8. PubMed PMID: 20102732.
2. Wang J, Mullighan CG, Easton J, Roberts S, Heatley SL, Ma J, et al. CREST maps somatic structural variation in cancer genomes with base-pair resolution. Nature methods. 2011 Aug;8(8):652-4. PubMed PMID: 21666668. Pubmed Central PMCID: 3527068.